**Ab Initio Modeling of MultiWall: A General Algorithm First Applied to Carbon Nanotubes**

# Ab initio Modeling of Multi-Wall: a general algorithm first applied to carbon nanotubes



| | |
|---|---|
| Journal: | *The Journal of Physical Chemistry* |
| Manuscript ID | jp-2021-01682m.R2 |
| Manuscript Type: | Article |
| Date Submitted by the Author: | n/a |
| Complete List of Authors: | Marana, Naiara; UNESP,<br>Noel, Yves; UPMC, Lab PMMP<br>Sambrano, Julio; Unesp, Universidade Estadual Paulista, Matematica<br>Ribaldone, Chiara; UNITO, Chemistry<br>Casassa, Silvia; Universita degli Studi di Torino, Dipartimento di Chimica IFM |
| | |

# Ab Initio Modeling of Multi-Wall: a General Algorithm First Applied to Carbon Nanotubes

Naiara Leticia Marana[a,c], Yves Noel[b], Julio Ricardo Sambrano[a], Chiara Ribaldone[c], Silvia Casassa[*,c]

[a] *Modeling and Molecular Simulation Group - CDMF, São Paulo State University, UNESP, Bauru, SP, Brazil*
[b] *Institut des Sciences de la Terre Paris (iSTeP), Sorbonne Université, Paris, France*
[c] *Theoretical Group of Chemistry, Chemistry Department I.F.M., Torino University, Torino 10124, Italy*

**Abstract**

A general, versatile and automated computational algorithm to design any type of multi-wall nanotubes of any chiralities is presented for the first time. It can be applied to rolling up surfaces obtained from cubic, hexagonal and orthorombic lattices. Full exploitation of the helical symmetry permits a drastic reduction of the computational cost and therefore opens to the study of realistic systems. As a test case, the structural, electronic, mechanical and transport properties of multi-wall carbon nanotubes ($MWCNT$) are calculated with a Density Functional Theory approach and results are compared with those of the corresponding layered (graphene-like) precursors.

The interaction between layers has a general minimum for the inter-wall distance of $\approx 3.4$ Å , in good agreement with experimental and computed optimal distance in graphene sheets. The metallic *armchair* and semiconductor *zigzag* $MWCNT$ are almost iso-energetic and their stability rises up as the number of walls increases. The vibrational fingerprint provides a reliable tool to identify the chirality and the thickness of the nanostructures. Finally, some promising thermoelectric features of the semiconductor $MWCNT$ are reproduced and discussed.

*Corresponding author
*Email address:* silvia.casassa@unito.it (Silvia Casassa)

*Key words:* multi-wall nanotube, DFT, CNT, thermoelectrics

## 1. Introduction

In the last decades, with the advancement of nanotechnology, different structures emerged, characterized by promising and appealing properties. Such structures boosted the progress in material sciences and fostered not only the research but also the application of nanomaterials in the most diverse areas, from medicine to electronic devices.[1]

Alongside the synthesis and the experimental characterization of such materials, the development of reliable computational tools can be a good way to asses their fundamental properties and exploring the effects of chiaralities, thickness and doping process to obtain a preliminary screening of potentially interesting systems for technological and scientific applications.

With this goal, in 2010, Noel and coworkers[2] implemented in the CRYSTAL program an original algorithm which fully exploits the helical symmetry in a periodic contest and allows the modeling and simulation of single-wall nanotubes.[3] In particular, by defining very few input parameters it is possible to design nanotubes of any diameter and chirality, starting from slabs and/or bulk of different materials. The ability of the code to deal with the ground state properties, its accuracy and generality has been widely demonstrated.[4, 5, 6, 7] Moreover, more recently, ZnO/AlN/GaN nanotubes have been fully characterized with respect to their reactivity towards small molecules of catalytic interest.[8, 9, 10] Unfortunately, this method only allowed single-wall modeling. Double-wall nanotubes have been conveniently conceived by wrapping a double-layers slab[11, 12] but in this kind of strategy, the structure is subjected to a strain due to the wrapping procedure that elongates the bonds and deforms the bond angles. This deformation effect can lead to the calculation of incorrect or unrealistic properties. Furthermore, the extension to systems with more than two walls is neither direct nor general. As far as we know, few other studies have been done on multi-wall ($MW$) systems,[13, 14] perhaps for this very reason.

Experimentally, $MW$ nanotubes are routinely synthesized and studied. On the one hand, a greater thickness can be deliberately sought to increase the strength of the material and improve its performance. On the other, it can be difficult to control the wall growth during the synthesis process so that many nanotubes may have a thickness of a few nanometers, which corresponds to some walls.

To fill the gap between theory and experiment and to turn the research in nanotubes more effective it would be desirable a tool to design, manipulate and computed $MW$ nanotubes. Hence, the above algorithm was extended by Y. Noel, based on an original scheme proposed by R. Dovesi, to address $M$-wall nanotubes ($M \geq 2$) obtained by wrapping any type of layered material in different chiralities. This new tool takes full advantage of the entire machinery and features of the CRYSTAL package, especially as regards the use of symmetry, with a great saving of time and computational resources and the consequent ability to completely characterize large systems.

As a first application, we underwent the study of multi-wall carbon nanotubes, $MWCNT$, as a prototype of a material of both scientific and technological interest.

Carbon nanotubes[15, 16] ($CNT$) have many potential applications in different fields, including biomedical sensor, storage and energy conversion devices, nanoscale molecular sieves, additives for polymeric bracket materials in catalytic processes, etc.[17, 18, 19]. Their synthesis is often accompanied or directed to the formation of multi-wall structures, $MWCNT$. These can have some characteristics similar to those of the single-wall but with greater structural stability and uniformity. Or they may have specific peculiarity, such as a lower thermal conductivity,[20, 21] which make them interesting materials from the point of view of technological applications, in this case as thermoelectric materials.[22] So, in documenting and exploring the limitations and potential of the new tool, we have also provided a first glimpse of challenging problems such as the spectroscopic characterization of $MWCNT$ and the engineering of semiconductor

$MWCNT$s to be exploited in thermoelectric devices.

The manuscript is structured as follows: in the next Section the method to model nanotubes is revised and generalized to the case of multi-wall systems. Then, the algorithm is tested on different kind of $MWCNT$ which are characterized as regards their structural, electronic, dynamical and transport properties. Results are compared with the experimental and/or theoretical data, when available in literature.

## 2. Methods

### *2.1. Theory*

CRYSTAL is a computational tool for solid state chemistry and physics based on an original expansion of the crystalline wave function into a set of localized Gaussian-type orbitals, centered on each atoms of the unit cell. Hartree-Fock (HF), density functional theory (DFT), and hybrid methods are available at a low computational cost due to a fully exploitation of point and translational symmetry, both in the direct and reciprocal space. In addition, CRYSTAL can deal, at the same level of accuracy, with different dimensions ($D$): $0D$ (molecules and polymers) $1D$ (nanotubes and nanowires) $2D$ (surfaces) and $3D$ (bulk). As regards nanotubes, the use and exploitation of the additional helical symmetry has provided a double benefit: (i) a particularly friendly and simple *input* and (ii) the possibility to simulate very large tubes.

Nanotubes are cylindrical structures periodic along a single direction, usually defined as $x$. They can be modeled by wrapping the corresponding $2D$ layer along the rolling vector, $\mathbf{R}$, defined as $\mathbf{R} = n_1\,\mathbf{a_1} + n_2\,\mathbf{a_2}$ where $\mathbf{a_1}$ and $\mathbf{a_2}$ are the lattice vectors of the slab unit cell and $(n_1, n_2)$ are integer numbers that fully define the nanotube. In fact, $|R|$ is the circumference and the chiral angle, $\theta$, is defined as the angle between $\mathbf{R}$ and $\mathbf{a}_1$.[23] According to Hamada[24], the chirality can be defined as follows: armchair $(n_1, n_1)$, zigzag $(n_1, 0)$ or chiral $(n_1, n_2)$. So, from $\mathbf{R}$, the nanotube diameter $D = |R|/\pi$ and the angle $\theta$ can be

calculated as

$$D = \frac{\sqrt{3}\, d\, \sqrt{n_1^2 + n_1\, n_2 + n_2^2}}{\pi} \quad (1)$$

$$\cos(\theta) = \frac{2n_1 + n_2}{2 \times (\sqrt{n_1^2 + n_1\, n_2 + n_2^2})} \quad (2)$$

where $d$ is the C-C bond length. Then, depending on $\mathbf{R}$, two other lattice vectors are uniquely defined in terms of 4 integers: (i) the nanotube lattice parameter $\mathbf{L}$, chosen as the shortest vector perpendicular to $\mathbf{R}$ and defining the periodicity along $x$: $\mathbf{L} = l_1\mathbf{a_1} + l_2\mathbf{a_2}$ (with $l_1$ and $l_2$ integers); (ii) the helical (i.e. roto-translational) vector $\mathbf{H} = h_1\mathbf{a_1} + h_2\mathbf{a_2}$, which posses a rotational component along the circumference vector, $\mathbf{R}$, and a translational component along the lattice parameter, $\mathbf{L}$, and then determines the correspondence between a translation in the flat slab with a roto-translation on the curved surface.

The periodicity along the tube axis, i.e. the existence of the longitudinal vector $\mathbf{L}$, is not satisfied for all possible $2D$ (slab) lattices. In fact, the orthogonality condition between $\mathbf{R}$ and $\mathbf{L}$ provides the following equation:

$$\begin{aligned} \mathbf{R}\cdot\mathbf{L} &= (l_1\mathbf{a_1} + l_2\mathbf{a_2})\cdot(n_1\mathbf{a_1} + n_2\mathbf{a_2}) = \\ &= n_1 l_1 |a_1|^2 + n_2 l_2 |a_2|^2 + (n_1 l_2 + n_2 l_1)|a_1||a_2|\cos\gamma = 0 \end{aligned} \quad (3)$$

However, this equation cannot be satisfied for any combinations of $\mathbf{a_1}, \mathbf{a_2}$, and $\gamma$. The equation generates the $l_1/l_2$ ratio, which is a rational number, whereas $\cos\gamma$ and $\mathbf{a_1}, \mathbf{a_2}$ are real numbers. This is the reason why, among the five $2D$ Bravais lattices, the hexagonal and square ones are the only that can be wrapped in any chirality $(n_1, n_2)$ whereas rectangular and rhombohedral can only give rise to $(n_1, n_1)$ and $(n_1, 0)$ nanotubes, respectively, and it is not possible to roll up any tube starting from an oblique lattice.[25]

Starting from the same theory used for the single-wall nanotubes, the implementation of the multi-wall nanotubes follows. The novelty consists in the possibility to generate $M$ separately single-wall tubes, starting from a given $2D$ (or $3D$ by cutting the proper slab) system, according to the rules just outlined, as shown if Fig. 1. That is, once the rolling vector $\mathbf{R}$ of each wall is defined, the

code calculates the corresponding **L** and **H** vectors and from the atoms in the asymmetric unit generates the full nanotube.

The self consistent field (SCF) cycle becomes a double-step procedure: first, the wave function of each wall, with its own symmetry, is calculated; then, eventually using as initial guess the density matrix just calculated for each tube, the energy of the whole multi-wall structure is computed. In the last step, only common symmetry operators are kept. For sake of clarity, the corresponding *input* examples are given in Table. S1 of the Supplementary Information (SI).

As regards the geometry optimization, two procedures have been implemented. The first, ruled by the *OPTWALL* keyword, is a full optimization (atomic coordinates, cell parameters and volume) of each wall, as a separate moiety. Therefore, with this option, each wall is relaxed as if it were isolated. The second, controlled by the keyword *OPTMULTI*, performs a complete optimization of the entire multi-wall system and only the common symmetry operators (if any) are retained along the process. The two strategies, documented in Table S2, can be used together in the search for the minimum energy configuration, potentially saving a lot of CPU time.

Besides that, nanotubes walls can be manipulated and reoriented one respect to the others using two new keywords. *ROTWALL* allows to rotate the nanotubes wall of any angle between 0° and 360° along the periodic axis, $x$. *TRANSWALL* performs a rigid shift of the atomic position of the selected wall along the $x$-axis. Both options can be used in association with the optimization keywords in order to optimize the inter-layer stack. *Input* examples are reported in Table S3.

### *2.2. Computational Set Up*

The calculations are performed with a $\beta$ version of the CRYSTAL code, using both the generalized gradient approximated Perdew-Burke-Ernzerhof functional[26] (PBE) and the global hybrid B3LYP[27] which includes 20% of the exact exchange. In order to account for dispersion, the B3LYP-D3 functional as originally proposed by Grimme[28] and implemented in the code, is also employed.

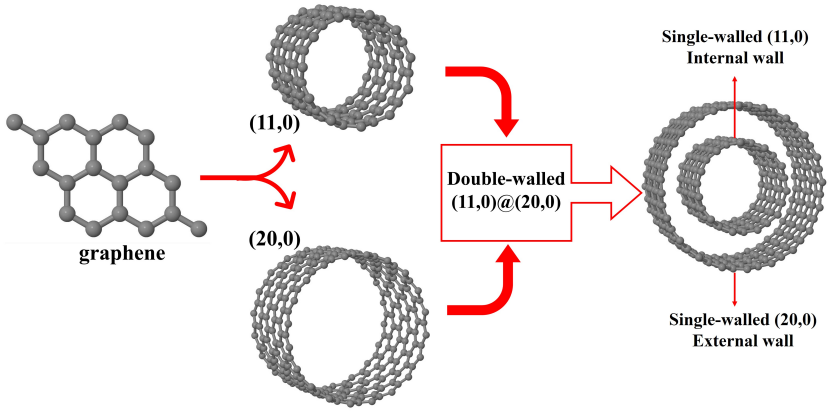


Figure 1: Rolling up a multi-wall nanotube structure with CRYSTAL.

Carbon atoms are described by the standard all-electron basis set 6-21G*.[29]

The DFT integration is performed within a grid containing 99 radial and 1454 angular points, as specified by the XXLGRID keyword.[30] The accuracy of the truncation criteria for the bi-electronic integrals, Coulomb and HF exchange series, is controlled by a set of five thresholds for which the strict values of [8, 8, 8, 8, 16] are adopted. In the self-consistent field procedure (SCF) the shrinking factor for both the diagonalization of the Fock matrix and the calculation of the energy is set to 4, corresponding to 4 independent **k**-points in the irreducible part of the Brillouin zone. The total and projected density of state (DOS) and the band structure are plotted using the same **k**-point sampling as in the SCF. The vibrational frequencies at the Γ point were computed within the harmonic approximation by diagonalizing the mass-weighted Hessian matrix.[31, 32] Intensities were evaluated with a Berry phase approach through the calculation of the atomic Born tensors and the corresponding IR spectra are produced using a Lorentzian shape with a FWHM of 10 $cm^{-1}$ attributed to each peak.[33]

The Seebeck coefficient ($S$) and the power factor ($PF$) of semiconductors $MWCNT$ were calculated using the semi-classical Boltzmann transport equation theory[34] (BTE) the frozen band approximation and assuming the energy

relaxation time for carriers a constant parameter, derived on the basis of experimental measurements.[35]

Carbon nanotubes are obtained from the rolled-up of a single sheet of graphite, i.e. graphene. Graphite belongs to the hexagonal space group $P6_3/mmc$ with unit cell parameters $\mathbf{a} = 2.47$ $\AA$ and $\mathbf{c} = 6.60$ $\AA$, and consists of flat layers of hexagons of carbon atoms. In each layer, the $sp^2$-hybridized carbon atoms are covalently bonded to three other carbon atoms. Starting from the graphite bulk it is possible to cut a one-layer slab, orthogonal to the **c** axes, characterized by the four Miller indexes [0001] and roll it up to design nanotubes of any chirality. As an alternative, carbon nanotubes can be wrapped starting from the slab, belonging to the point group $\mathrm{P}_{6mm}$ with cell parameter $\mathbf{a} = 2.47$ $\AA$. The input files for both possibilities are reported in Table S1.

It is worth to note that *CNT* are usually built starting from an hexagonal cell, with $\gamma = 60°$, whereas the adopted convention in CRYSTAL is $\gamma = 120°$ and this has to be carefully considered in the choice of the $n_1$ and $n_2$ parameters that define the **R** rolling vector.[2]

Multi-wall carbon nanotubes ($MW$) are used as a test case to verify the reliability of the implemented algorithm and explore the generality of the method. Calculations were performed on a set of double-wall systems, $DW$, considering tubes obtained from both the bulk and the slab and with different chiralities, i.e. *armchair*, *zigzag* and *chiral*. Then, in order to investigate the influence of the number of walls on the electronic structure and mechanical properties, starting from the most stable *armchair* and *zigzag* double-wall systems, a set $MW$s of increasing diameter, with $M > 2$, has been designed and characterize.

Graphene, $gr$, and the corresponding single-wall tubes, $SW$, were simulated and optimized at the same computational level to allow a fruitful and unavoidable comparison. In particular, the multi-wall stability is discussed according to the following two quantities. The formation energy per atom, $E_{\mathrm{form}}$, defined as the energy difference with respect to an optimized $M$-layers slab of graphene

$$E_{\mathrm{form}} = \frac{E(MW)}{n_{MW}} - \frac{E(Mgr)}{n_{Mgr}} \quad (4)$$

where $E(MW)$ and $E(Mgr)$ are the energies of the optimized $M$-wall nanotube and $M$-layer graphene, respectively, and $n_x$ are the number of atoms in the corresponding reference cells. And the inter-wall energy, $E_{\rm iw}$, which is an estimate of the interaction between walls, normalized on the number of walls, $M$:

$$E_{\rm iw} = \frac{1}{(M-1)}\left[\frac{E(MW)-\sum_M E_M(SW)}{n_{MW}}\right] \quad (5)$$

where $E_M(SW)$ are the energies of the isolated single wall nanotubes. In this case, an estimate of the basis set superposition error (BSSE) is provided adopting the counterpoise method, proposed in the 70's by Boys and Bernardi.[36, 37] The corrective term, $E_{\rm BSSE}(SW)$, is calculated for each wall

$$E_{\rm BSSE}(SW) = \frac{E(SW_{\rm f})-E(SW_{\rm f})^{ghosts}}{n_{SW}} \quad (6)$$

and added to $E_{\rm iw}$. The two quantities in the equation above refer to the energy of the single nanotube frozen in the final $MW$ optimized geometry, isolated, $E(SW_{\rm f})$, and surrounded by ghost functions placed in the same position of the other walls, $E(SW_{\rm f})^{ghosts}$ respectively.

## 3. Results and Discussion

### *3.1. Internal check*

After several tests on different structures, based of their relative stability we have selected three double-wall carbon nanotubes, namely (7, 7)@(12,12), (12, 6)@(20, 10) and (11,0)@(20,0) as the representative of different chiralities, see Table 1. The internal consistency and the accuracy of the computational scheme were verified by exploring the following possibilities: ($A$) tubes are built starting from the 3D *or* 2D precursor; ($B$) relaxed or *un*relaxed $M$-layers are used as a starting point; ($C$) the two optimization procedures ($OPTWALL$+$OPTMULTI$ *vs* $OPTMULTI$) are compared.

The three strategies provide the same final results in terms of total energy, atomic positions and lattice parameter, band gap ($E_{\rm gap}$) and Mulliken charges. The difference is in the required CPU time which for the present simple models

is not essential but can become crucial when hundreds or thousands of atoms are involved. It is worth to say that the very high symmetry characterizing each tube, that is fully exploited during the $OPTWALL$ procedure, is generally lost in the $MW$ calculation in which few (if any) symmetry operators are retained.

As regards (C) tests, the two optimization procedures provide equivalent results, as documented in Fig. S1 and the $OPTWALL + OPTMULTI$ option results the most time-efficient.

Finally, the $TRANSWALL$ and $ROTWALL$ options, which can become a useful tool for materials with more complex structures that may require elaborate modeling, were tested. In the case of carbon wall nanotubes, the possibility of exploring these further degrees of freedom is particularly interesting because of the well know influence of the interlayer stacking on the main properties of graphene-like materials.[38, 39]

The translation along the periodic axis occurs without any energy barrier, both at the PBE and B3LYP-D3 level. Instead, by rotating the outer wall of the *armchair* (7,7)@(12,12) and of the *zigzag* (11,0)@(20,0) nanotubes between -4.3 and 4.3 degrees, we obtained the energy curves of Fig. 2. This angle represents the difference in degrees between two equivalent inner/outer-wall configurations. In the case of *armchair* (*zigzag*) a rotation of 2° yields a configuration 0.05 (0.03) eV more stable that the starting one, indicating that a favorable stacking of the layers can significantly stabilize the structure.

### *3.2. Structures and energies*

The first set of calculations was performed on double-wall nanotubes ($DW$) exploring the three chiralities, *armchair*, *zigzag* and *chiral*, and the effect of the inter-wall distance. The main results are collected in Table 1.

In general, the distortion with respect to graphene is uniformly distributed over all the atoms of the lattice as imposed by symmetry. Bond angles and distances deviate by only a small amount from those of the planar geometry. In particular, the distances between adjacent carbon atoms are in range 1.42 - 1.47 Å while in the two-layers of graphite the average C-C length is 1.43 Å.

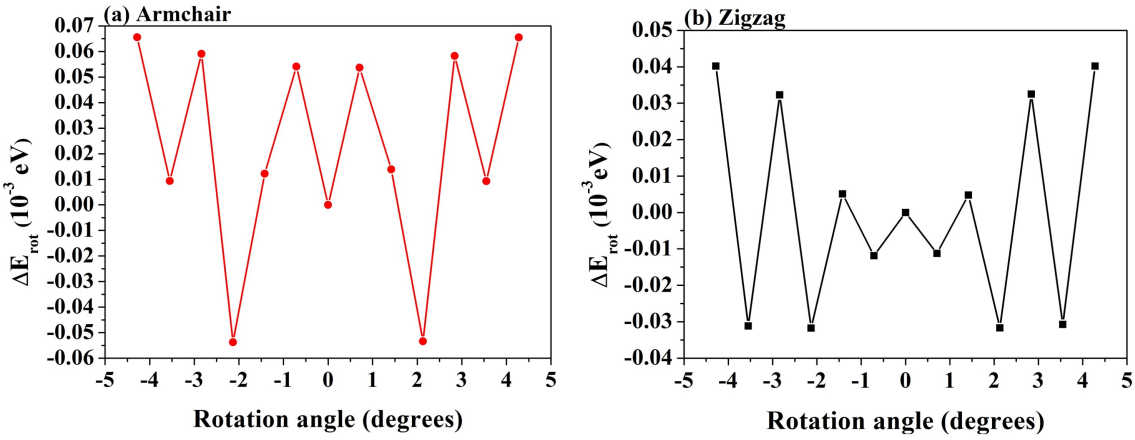


Figure 2: Energy dependence (PBE, in meV) on the orientation of outer tube. The same trend is calculated at the B3LYP-D3 level. (left) and (right) panels represent the *armchair* (7,7)@(12,12) and *zigzag* (11,0)@(20,0) *DW* when the outer wall is rotated between -4.3° < $\gamma$ < 4.3° while the inner wall is kept fixed.

The $\widehat{CCC}$ angles present small deviation from the ideal value of 120°.

The effect of symmetry on the CPU time is evident when comparing the (6,6)@(12,12) and (7,7)@(12,12) *DW* which have 24 and 6 symmetry operators, respectively. Given the same number of SCF cycles to converge and a negligible difference in the number of atoms in the cell, it can be argued that the CPU speed-up is proportional to the ratio of the number of symmetry operators.

The formation energy of these systems is found as a balance between two contributions, the strain energy, defined as the force to wrap $M$-flat surfaces, and the inter-wall interaction. Regardless the functional adopted, $E_{\text{form}}$ is always positive indicating that a given amount of energy is needed to synthesized these materials starting from their 2D precursor. As expected, the less stable structures, with higher $E_{\text{form}}$, are those with the smallest inter-wall distance and the most distorted geometries in terms of bond lengths and angles.

Interesting enough, the two structures with the lowest formation energy, the *armchair* (7,7)@(12,12) and the *zigzag* (11,0)@(20,0) have an interlayer distance of $d_{\text{iw}}$=3.46 and 3.63 Å respectively. These values are extremely close to that of 3.35 Å measured in graphite[40] and of 3.48 Å recently determined for bilayer

| | $n_{AT}$ | C-C | $\hat{C}$ | $d_{\rm IW}$ | $D_{\rm in}$ | $D_{\rm ext}$ | $E_{\rm gap}$ | $E_{\rm form}$ | $n_{\rm sym}$ | $n_{\rm cyc}$ | CPU |
|---|---|---|---|---|---|---|---|---|---|---|---|
| **Armchair** | | | | | | | | | | | |
| (6,6)@(12,12) | 72 | 1.43 | 119.6 | 4.08 | 8.28 | 16.44 | 0.0 | 0.062 | 24 | 7 | 806 |
| (7,7)@(12,12) | 76 | 1.43 | 119.7 | 3.46 | 9.69 | 16.48 | 0.0 | 0.056 | 4 | 10 | 5804 |
| (8,8)@(12,12) | 80 | 1.44 | 120.3 | 3.02 | 10.79 | 16.66 | 0.0 | 0.076 | 16 | 11 | 2490 |
| (9,9)@(12,12) | 84 | 1.44 | 119.7 | 2.06 | 11.79 | 17.35 | 0.0 | 0.162 | 12 | 14 | 5626 |
| **Zigzag** | | | | | | | | | | | |
| (10,0)@(20,0) | 120 | 1.43 | 119.9 | 3.93 | 7.95 | 15.81 | 0.45 | 0.080 | 40 | 12 | 2650 |
| (11,0)@(20,0) | 124 | 1.43 | 120.0 | 3.63 | 8.76 | 15.84 | 0.34 | 0.076 | 4 | 13 | 10494 |
| (12,0)@(20,0) | 128 | 1.43 | 120.1 | 3.26 | 9.47 | 15.84 | 0.07 | 0.085 | 32 | 33 | 6281 |
| (13,0)@(20,0) | 132 | 1.45 | 119.1 | 3.03 | 10.16 | 16.09 | 0.02 | 0.095 | 4 | 15 | 23277 |
| (15,0)@(20,0) | 140 | 1.47 | 121.5 | 2.81 | 11.37 | 16.78 | 0.00 | 0.200 | 20 | 25 | 11345 |
| **Chiral** | | | | | | | | | | | |
| (6,12)@(10,20) | 448 | 1.43 | 119.7 | 4.16 | 12.57 | 20.89 | 0.11 | 0.043 | 8 | 11 | 450176 |
| (7,14)@(10,20) | 476 | 1.42 | 121.0 | 3.12 | 14.56 | 20.80 | 0.16 | 0.050 | 2 | 13 | 1460165 |

Table 1: Structural properties of the armchair and zigzag double-wall nanotubes. Number of atoms ($n_{AT}$) bond length (C-C) bond angle ($\hat{C}$) inter-wall distance ($d_{\rm IW}$) internal and external diameters ($D_{\rm in}$ and $D_{\rm ext}$) fundamental energy gap, $E_{\rm form}$ at the PBE level, number of symmetry operators ($n_{\rm sym}$) are reported. Distances are in $\AA$, angles in degrees and energies in eV. For a single SCF the number of cycle, $n_{\rm cyc}$, and the total CPU time, in seconds, on 16 processors of an Intel Xeon 3.00GHz cluster, are reported.

graphene[41] and only slighter longer than the experimental inter-wall distances of 3.41-3.35 Å observed for multi-wall carbon nanotubes by Saito et al..[42] The good agreement with the experimental data confirms that the algorithm is able to predict the most likely structures. It can therefore be concluded that (7,7)@(12,12) and (11,0)@(20,0) double-wall systems are almost iso-energetic so that both *armchair* and *zigzag* chiralities can be obtained, as already stated in a previous work on single-wall carbon nanotube[9] and confirmed by several experimental findings.[43]

Then, starting from (7,7)@(12,12) and (11,0)@(20,0), two sets of nanotubes

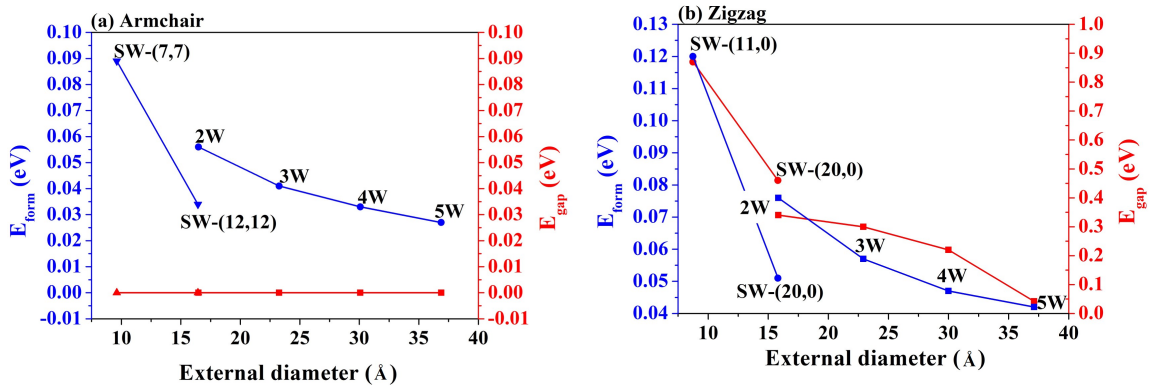


Figure 3: $E_{\mathrm{form}}$ at the PBE level, for *armchair* and *zigzag* *MW* nanotubes of increasing number of walls. For both chiralities, $E_{\mathrm{gap}}$ as a function of the outer wall diameter is also reported (red curves).

up to 5 walls, of increasing outer diameter, are drawn, keeping the distance between the walls equal to the optimal value of $d_{\mathrm{iw}}$ 3.46 and 3.63 Å for armchair and zigzag, respectively. Structural details are reported in Tab. S5. The largest $5W$ tubes have a diameter of $\approx 37$ Å, already in the order of some synthesized experimental samples.[44, 45] The formation energies, computed according to Eq. 4, using a fully optimized $M$-layer sheet of graphite as reference system, is shown as a function of the $MW$ diameter in Fig. 3. In accordance with experimental observation, $E_{\mathrm{form}}$ decreases as the number of walls increases. For the largest *armchair* and *zigzag* systems, containing 340 and 580 atoms in the reference cell, respectively, $E_{\mathrm{form}}$ is 0.03 and 0.04 eV/per atom.

Finally, to explore the inter-wall interaction as a function of the inter-wall distance, it was designed a set of *armchair* (7,7)@(X,X) characterized by outer walls at increasing distance, ranging from $d_{\mathrm{iw}} = 2.85$ (for X=11) to $d_{\mathrm{iw}} = 15.8$ (for X=30). Structural and energetic details of this *DW* family, as evaluated at the PBE, B3LYP and B3LYP-D3 level, are reported in Table 2. For all functionals, the BSSE correction does not change neither the general trend either the position of the minimum, resulting negligible for inter-wall distances

up to 5 Å. The inter-layer distances, as evaluated at the B3LYP-D3 level, are slightly shorter than in the PBE and B3LYP geometries. On the contrary, the functional adopted is crucial in determining the correct energy balance of these structures. As expected, an attractive inter-layer interaction is calculated only at the B3LYP-D3 level, confirming the fundamental role played by the dispersive forces in these materials.

| | | PBE | | | B3LYP | | | B3LYP-D3 | | |
|---|---|---|---|---|---|---|---|---|---|---|
| | $n_{AT}$ | $d_{\mathrm{IW}}$ | $E_{\mathrm{form}}$ | $\mathrm{E}_{\mathrm{iw}}^{BSSE}$ | $d_{\mathrm{IW}}$ | $E_{\mathrm{form}}$ | $\mathrm{E}_{\mathrm{iw}}^{BSSE}$ | $d_{\mathrm{IW}}$ | $E_{\mathrm{form}}$ | $\mathrm{E}_{\mathrm{iw}}^{BSSE}$ |
| @(11,11) | 72 | 3.01 | 0.089 | 0.0568 | 2.96 | 0.080 | 0.0747 | 2.89 | 0.056 | -0.0119 |
| @(12,12) | 76 | 3.41 | 0.056 | 0.0155 | 3.51 | 0.034 | 0.0203 | 3.40 | 0.030 | -0.0221 |
| @(13,13) | 80 | 4.11 | 0.050 | 0.0024 | 4.07 | 0.031 | 0.0119 | 3.38 | 0.039 | -0.0193 |
| @(14,14) | 84 | 4.76 | 0.049 | 0.0001 | 4.94 | 0.021 | 0.0007 | 4.74 | 0.049 | -0.0109 |
| @(15,15) | 88 | 5.63 | 0.046 | 0.0002 | 5.44 | 0.018 | 0.0003 | 5.47 | 0.051 | -0.0059 |
| @(16,16) | 92 | 6.13 | 0.044 | 0.0002 | 6.13 | 0.015 | 0.0002 | 6.16 | 0.051 | -0.0035 |
| @(18,18) | 100 | 7.51 | 0.040 | 0.0001 | 7.49 | 0.010 | 0.0001 | 7.48 | 0.049 | -0.0014 |
| @(20,20) | 108 | 8.85 | 0.036 | 0.0000 | 8.93 | 0.007 | 0.0001 | 8.83 | 0.046 | -0.0006 |
| @(30,30) | 148 | 15.83 | 0.026 | 0.0000 | 15.91 | 0.001 | 0.0000 | 15.65 | 0.003 | 0.0000 |

Table 2: The (7,7) tube contains 28 carbon atoms. Number of atoms, $n_{AT}$, inter-wall distance, $d_{\mathrm{IW}}$, $E_{\mathrm{form}}$ and inter-wall energy BSSE corrected as evaluated at the PBE, B3LYP and B3LYP-D3 level are reported. Energies are in eV per atom.

### *3.3. One-electron properties*

Band structure and density of state of the most stable *DW* systems, namely the (7,7)@(12,12) and (11,0)@(20,0) are calculated and discussed with reference to the corresponding properties of the single-wall nanotubes. Results are summarized in Fig. 4.

In the case of *armchair SW* nanotubes there are two evident Dirac cones, one in the conduction and the other in the valence bands, that intersect each others in a single **k** point, determining the metallic behavior of these systems, see Fig. S3. In the *DW* structure the Dirac cones of the two nanotubes almost

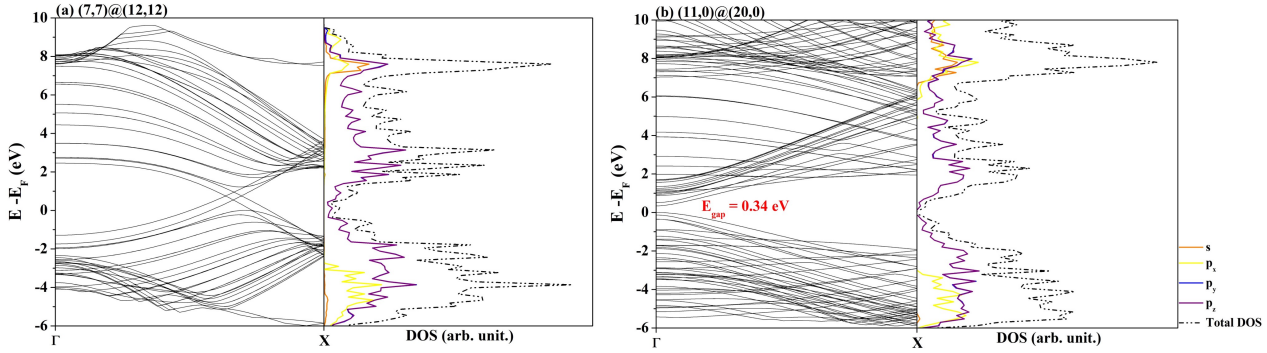


Figure 4: Band structure and density of states for *armchair* (7,7)@(12,12) (left) and *zigzag* (11,0)@(20,0) (right) *DW* nanotubes. The corresponding features for the single-wall tubes are reported in Fig. S3. To facilitate comparison, the bands have been shifted to bring the Fermi level of each system to coincide with zero.

overlap, giving rise to two points of intersection and an enhancement of the conductivity.

*SW*s *zigzag* present a band gap which decreases as the diameter of the tube increases. The resulting *DW* structure retains the semiconductor character although the $E_{\mathrm{gap}}$ is smaller than those of the two isolated tubes.

The projected density of state on the different atomic orbitals of the carbon atoms (PDOS) can provide useful information on the band composition around the Fermi surface. The $p_y$ and $p_z$ are symmetry equivalent and then their contributions are equal whereas $p_x$ is oriented along the periodic direction. Also in the case of PDOS, both the *armchair* and *zigzag* *DW*s conserve the main features of the *SW* constituents. In particular, $s$ shells contribute to the lowest part of the valence band, $p_x$ orbitals give their contribution to the region slightly higher in energy and the $p_y$ and $p_z$ are the ones responsible for the bands immediately below and above the Fermi level. These last bands determine most of the properties related to electronic mobility (chemical reactivity but also conductivity) and are indeed particularly interesting.

In the case of *zigzag* *MWCNT*, the band gap decreases as the number of walls rises up, ranging from 0.30 eV for $M = 3$ to 0.08 eV for $M = 5$, see

Table S5. The persistence of a semiconductor character in these rather stable nanostructures paves the way for the study of their transport properties and potential thermoelectric performance.

### *3.4. Lattice dynamics*

IR and Raman frequencies in Γ were calculated at the PBE level for two sets of nanotubes: the *armchair* [(7,7) and (12,12) *SW*, (7,7)@(12,12) and (7,7)@(12,12)@(17,17) *MW*] and the *zigzag* [(11,0) and (20,0) *SW*, (11,0)@(20,0) and (11,0)@(20,0)@(29,0) *MW*].

The first-order experimental Raman spectrum of carbon nanotubes exhibits a line at 1582 $cm^{-1}$, due to the stretching of the C-C bond.[46] Our calculated values, around 1520 and 1540 $cm^{-1}$ for *armchair* and *zigzag* respectively, are in rather good agreement with the experimental finding, see Fig. S5. The weak interactions between layers have almost no effect on *MW* Raman fingerprint, as can be seen from the coincidence between the *DW* and the single-wall signals. Furthermore, the difference between the two sets is below the numerical precision, that is why it is practically impossible to determine the chirality by calculating the Raman spectra of such materials.

The IR spectra for *armchair* and *zigzag*, shown in Fig. 5 and Fig. S4, are in qualitative good agreement with the experimental vibrational modes obtained by Kastner et al.[46] for carbon nanotubes. Transmission infrared spectra show one broad and asymmetric line at 1575 $cm^{-1}$ and a line at 868 $cm^{-1}$. Interesting enough, we find IR signals at 1550 and 680 $cm^{-1}$, only for the *armchair* nanotubes while the *zigzag* spectra show a single intense peak around 690 $cm^{-1}$. This substantially different spectral profile, whose shape is maintained as the number of walls increases, could allow the identification of the chirality of the nanotube without ambiguity.

Moreover, despite the low values of $E_{\mathrm{iw}}$, the spectral fingerprint of $2W$ and $3W$ tubes presents original features that could help determine the thickness of the nanostructures. In the *armchair* tubes, the signal corresponding to the wagging out-of-plane vibration of the carbon atoms (680 $cm^{-1}$ for *SW*) becomes

a doublet, and then a triplet, for the $2W$ and $3W$ multi-wall. In addition, in the region of the soft modes, two/three small but distinct peaks emerge at their respective single-wall signal. As regards the *zigzag* structures, new down-shifted signal(s) appear, corresponding to the same displacement of the carbon atoms, as occurs in the 2(3) tubes.

Summarizing, the IR spectroscopy can provide clear information on both chirality and thickness of $MW$ nanotubes.

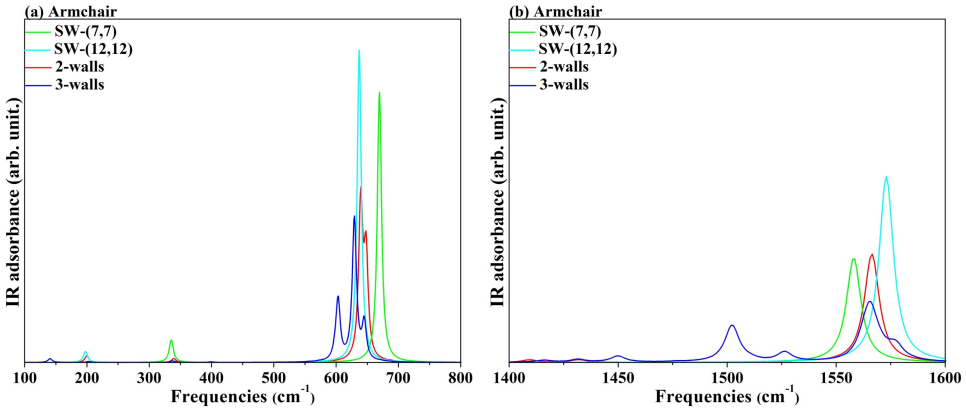


Figure 5: The IR spectra of 2 and 3 walls nanotubes, at the PBE level, are shown in the region of the soft modes (left panel) and high frequencies (right panel). The spectra of the single-wall (7,7) and (12,12) are added for comparison.

### *3.5. Transport properties*

We explored the thermoelectric performance of semiconducting $MWCNT$ in the frame of the Boltzmann transport formalism.[47] In order to validate our method and evaluate the effect of multiple walls on these properties, we first calculated the Seebeck coefficients for the $SWCNT$s. Results, shown in Fig. 6, can be summarized as follows: (i) $S$ increases with decreasing the diameter of the nanotube as a consequence of the narrowing of the band gap, in qualitative agreement with recent experimental results[48]; (ii) in accordance with theoretical predictions[49, 50] the peak of $S$ is nearly an order of magnitude higher than those observed experimentally.[51, 52] To comment on this discrepancy, it can

be noted that the Seebeck coefficient is highly sensitive to the position of the Fermi energy, which in turn is controlled by the carrier density. A small shift toward lower values of the chemical potential provides values for the thermopower in the range of the experimental findings. In particular, Nakai et al.[48] found a positive sign for $S$, indicating hole-like carriers and a value of $\approx 170 \mu V K^{-1}$ for $SWCNT$ with a mean diameter of $\approx 20$ Å. Our (29,0) tube has a diameter of 23 Å and the calculated thermopower at 300 K is $S \approx 280 \mu V K^{-1}$ for a chemical potential 50 meV lower than that of the Fermi level.

Then, we compute the Seebeck coefficient for the $MWCNT$. As measured in several samples, we found that the thermopower is almost one order of magnitude lower than in $SW$. Moreover, as the number of wall increases, the progressive narrowing of the gap causes a fall of $S$ with the consequent disappearance of any thermoelectric power. Both these features are documented in Fig. 7, where $S$ is reported for *zigzag* multi-wall, with $M > 4$, at 300 K. In the inset, the thermopower of the double-wall is compared with that of the constituents $SW$. The most interesting system seems to be the double-wall (11,0)@(20,0). Its thermoelectric behavior shows interesting features which partially reproduce the experimental results of Miao et al..[22] The dependence of $S$ and of the power factor on temperature is well reproduced and is shown in Fig. 8: as T rises up, the Seebeck coefficient decreases while the $PF$ increases slightly. Moreover, the value of $S$, in correspondence with the maximum of $PF$, which occurs for a chemical potential of -4.7 eV, is 36.7 $\mu V K^{-1}$, a value that is within the experimental range of 40-30 $\mu V K^{-1}$ reported by Miao.[22]

Based on these preliminary results, interesting insights could be hypothesized which unfortunately fall outside the scope of this manuscript. In particular, investigate the effect of different chirality on the band gap and simulate the doping process which can significantly reduce the thermal conductivity with a sensitive improvement in the thermoelectric figure of merit.

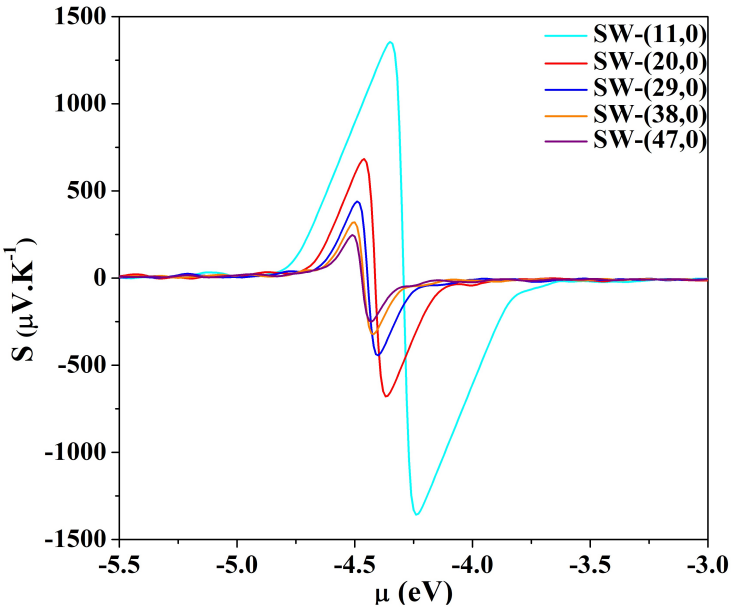


Figure 6: Seebeck coefficient at 300 K for *zigzag SW* nanotubes of increasing diameter. The peak value for (11,0) $S = 1300 \mu V K^{-1}$, is in perfect agreement with that calculated by Hung et al. for the same system[50].

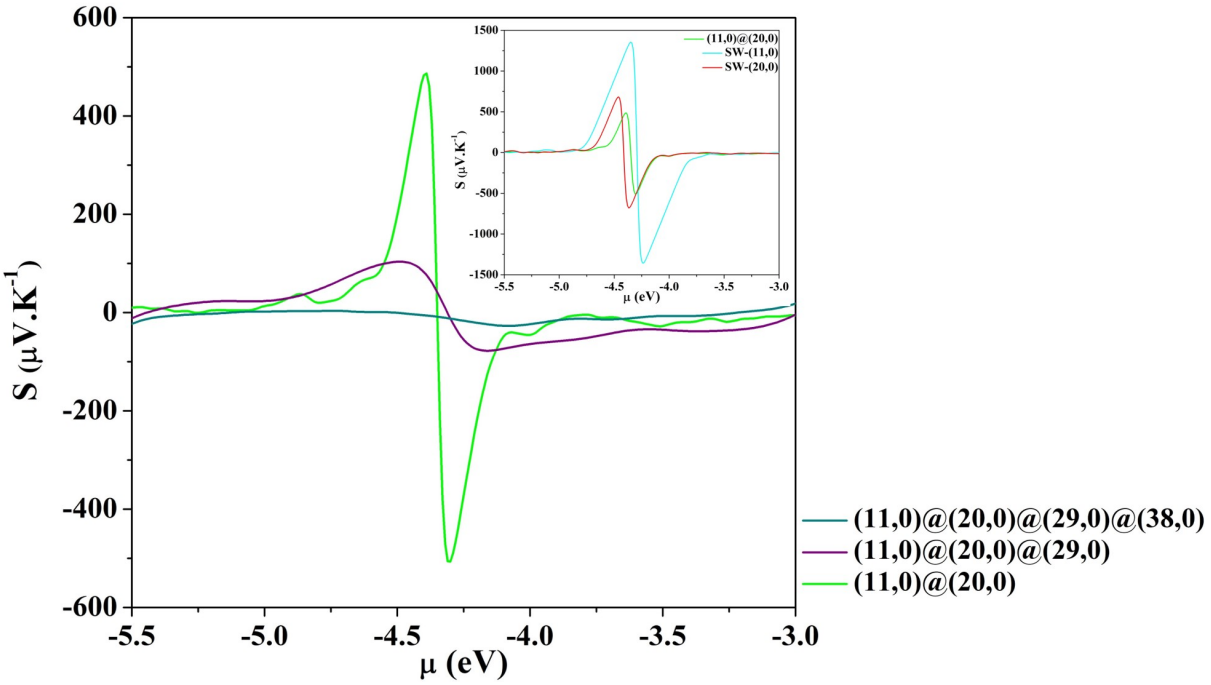


Figure 7: Seebeck coefficient at 300 K for *zigzag MW* nanotubes (11,0)@(20,0), (11,0)@(20,0)@(29,0) and (11,0)@(20,0)@(29,0)@(38,0). In the inset, the $S$ of (11,0)@(20,0) is compared with that of the two constituent tubes to highlight the different order of magnitude.

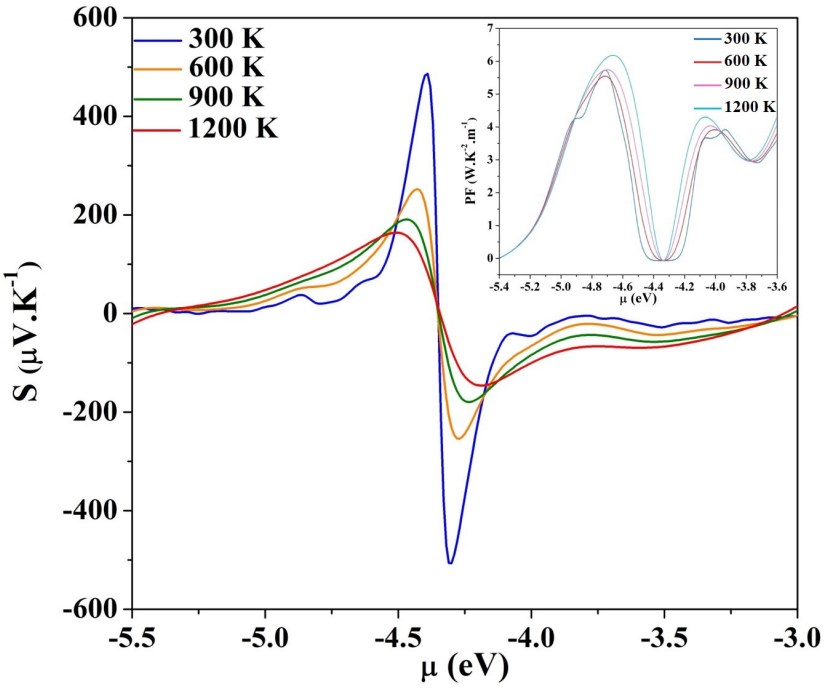


Figure 8: Seebeck coefficient of (11,0)@(20,0) at different temperatures. In the inset, the power factor at different temperature: its peak occurs at -4.7 eV, corresponding to a carrier concentration of $4 \cdot 10^{22}$ cm$^{-3}$.

## 4. Conclusions

In this manuscript, it is presented a general purpose robust scheme to model multi-wall nanotubes by rolling up layers cutting from hexagonal, square and rectangular lattices. The entire set of the CRYSTAL[3] features can be conveniently used to characterize these 1-dimensional periodic materials and to explore their potential technological applications. The full exploitation of helical symmetry allows for a particular user-friendly input design, conveniently reduces the computational cost and permit the treatment of large systems. In addition, there is always the possibility to perform a consistent internal check of every computed properties with respect to their values in the precursor 2-dimensional materials.

The algorithm is applied for the first time to a family of systems of technological and scientific interest as the multi-wall carbon nanotubes.

This preliminary investigation has shown that by working on chirality, inter-wall distance and thickness (i.e. number of walls) it is possible to design rather stable semiconductors to be used as innovative materials for promising application in the field of carbon-nanotube-based thermoelectric devices.

## 5. Supporting Information

In the Supporting Information the following material is supplied: (i) input examples, (ii) a flowchart of the *MULTIWALL* option, (iii) band structure and density of state, IR and Raman spectra of single and multi-wall nanotubes and (iv) structural information on the multi-wall systems.

## 6. Acknowledgments

This work is supported by FAPESP (Fundação de Amparo à Pesquisa do Estado de São Paulo) Brazil (2016/25500-4, 2019/12430-6, 2013/07296-2).
The Authors are extremely grateful to the CINECA Supercomputing Center which supported the work by providing the computational resources through the ISCRA Class C Project, code HP10CWYR6N (EXMUWN2).

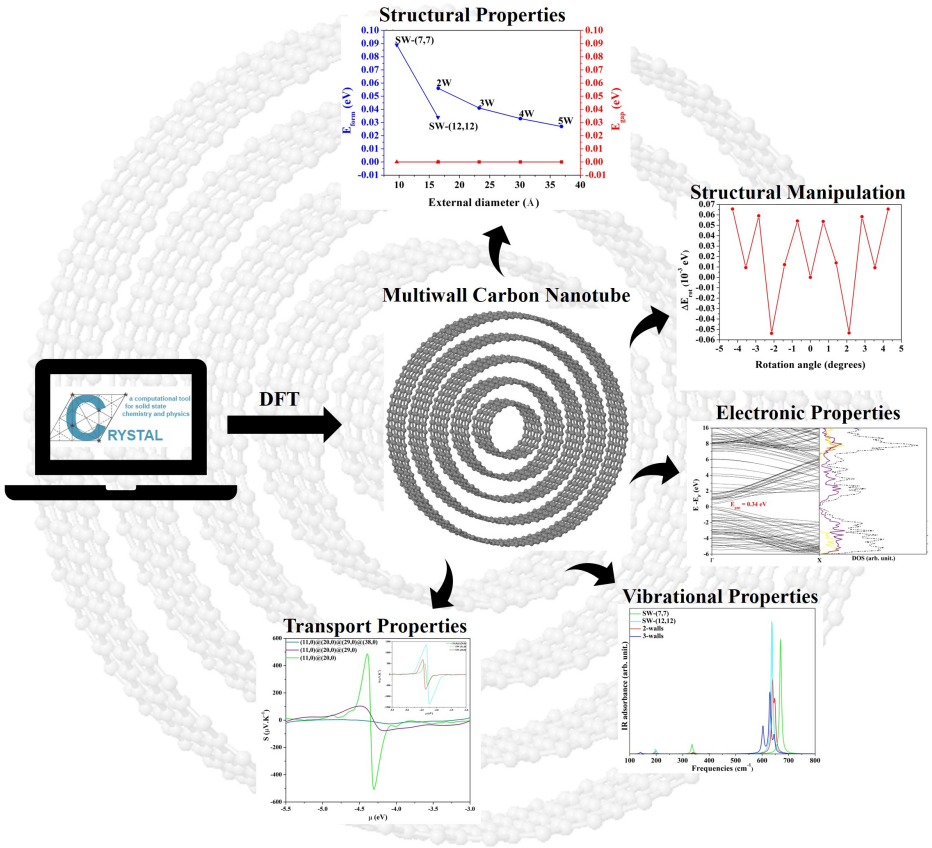


Figure 9: For Table of Contents Only.

## References


[1] L. A. Lalitha, I. V. K. Viswanath, B. S. Diwakar, B. Govindh, V. Reddy, Y. L. N. Murthy, Review on Nanomaterials: Synthesis and Applications, *Materials Today: Proceedings 18* (**2019**) 2182–2190.

[2] Y. Noel, P. D'Arco, R. Demichelis, C. M. Zicovich-Wilson, R. Dovesi, On the Use of Symmetry in the Ab Initio Quantum Mechanical Simulation of Nanotubes and Related Materials, *Journal of Computational Chemistry 31* (**2010**) 855–862.

[3] R. Dovesi, A. Erba, R. Orlando, C. M. Zicovich-Wilson, B. Civalleri, L. Maschio, M. Rérat, S. Casassa, J. Baima, S. Salustro, B. Kirtman, Quantum-mechanical Condensed Matter Simulations with CRYSTAL, *Wiley Interdisciplinary Reviews: Computational Molecular Science 8* (**2018**) e1360–96.

[4] P. D'Arco, Y. Noel, R. Demichelis, R. Dovesi, Single-layered Chrysotile Nanotubes: a Quantum Mechanical Ab Initio Simulation, *Journal of Chemical Physics 131* (**2009**) 204701–7.

[5] R. Demichelis, Y. Noël, P. D'Arco, L. Maschio, R. Orlando, R. Dovesi, Structure and Energetics of Imogolite: a Quantum Mechanical Ab Initio Study with B3LYP Hybrid functional, *Journal of Materials Chemistry 20* (**2010**) 10417–10425.

[6] A. M. Ferrari, D. Szieberth, C. M. Zicovich-Wilson, R. Demichelis, Anatase(001) 3 ML Nanotubes, The First TiO2 Nanotube With Negative Strain Energies: A DFT Prediction, *The Journal of Physical Chemistry Letters 19* (**2010**) 28542857.

[7] A. M. Ferrari, D. Szieberth, Y. Noël, DFT Modeling of Anatase Nanotubes, *Journal of Materials Chemistry* (**2011**) 4568–4580.

[8] V. Lacivita, A. Erba, Y. Noël, R. Orlando, P. D'Arco, R. Dovesi, Zinc Oxide Nanotubes: an Ab Initio Investigation of their Structural, Vibrational,

Elastic and Dielectric Properties, *The Journal of chemical physics 138* (**2013**) 214706–9.

[9] N. Marana, A. Albuquerque, F. La Porta, E. Longo, J. Sambrano, Periodic Density Functional Theory Study of Structural and Electronic Properties of Single-walled Zinc Oxide and Carbon Nanotubes, *Journal of Solid State Chemistry 237* (**2016**) 36–47.

[10] G. B. Pinhal, N. L. Marana, G. S. Fabris, J. R. Sambrano, Structural, Electronic and Mechanical Properties of Single-walled AlN and GaN Nanotubes via DFT/B3LYP, *Theoretical Chemistry Accounts 138* (**2019**) 31–42.

[11] N. L. Marana, G. B. Pinhal, J. A. S. Laranjeira, P. G. C. Buzolin, E. Longo, J. R. Sambrano, Strain-induced Novel Properties of Alloy Nitride Nanotubes, *Computational Material Science 177* (**2020**) 109589–8.

[12] N. L. Marana, S. Casassa, E. Longo, J. R. Sambrano, Computational Simulations of ZnO@GaN and GaN@ZnO Core@Shell Nanotubes, *Journal of Solid State Chemistry 266* (**2018**) 217–225.

[13] G. Giambastiani, S. Cicchi, A. Giannasi, L. Luconi, A. Rossin, F. Mercuri, C. Bianchini, A. Brandi, M. M, G. G. et al, Functionalization of Multiwalled Carbon Nanotubes with Cyclic Nitrones for Materials and Composites: Addressing the Role of CNT Sidewall Defects, *Chemistry of Materials 23* (**2011**) 1923–1938.

[14] G. Giambastiani, S. Cicchi, A. Giannasi, L. Luconi, A. Rossin, F. Mercuri, C. Bianchini, A. Brandi, M. M, G. G. et al, Investigation of the Mechanical Properties of Multi-Walled Carbon Nanotubes Using Density Functional Theory Calculations, *J. Computational and Theoretical Nanoscience 9* (**2012**) 980–985.

[15] S. Iijima, T. Ichihashi, Single-shell Carbon Nanotubes of 1-nm Diameter, *Nature 636* (**1993**) 603–605.

[16] D. S. Bethune, C. H. Klang, M. S. De Vries, G. Gorman, R. Savoy, J. Vazquez, R. Beyers, Cobalt-catalysed Growth of Carbon Nanotubes with Single-atomic-layer Walls, *Nature 636* (**1993**) 605–607.

[17] I. V. Zaporotskova, N. P. Boroznina, Y. N. Parkhomenko, L. V. Kozhitov, Carbon Nanotubes: Sensor Properties. A Review, *Modern Electronic Materials 2* (**2016**) 95–105.

[18] Y. Cao, S. Cong, X. Cao, F. Wu, Q. Liu, M. R. Amer, C. Zhou, Review of Electronics Based on Single-Walled Carbon Nanotubes, in: *Single-Walled Carbon Nanotubes: Preparation, Propertyand Application*, **2017**, pp. 375–450. doi:10.1007/978-3-030-12700-8_7.

[19] P. Sharma, N. Kumar Mehra, K. Jain, N. Jain, Biomedical Applications of Carbon Nanotubes: A Critical Review, *Current Drug Delivery 13* (**2016**) 796–817.

[20] Y. K. Kwon, P. Kim, Unusually high thermal conductivity in carbon nanotubes, *Physical Review Letters 84* (**2000**) 4613–4616.

[21] D. J. Yang, Q. Zhang, G. Chen, S. F. Yoon, J. Ahn, S. G. Wang, Q. Zhou, Q. Wang, J. Q. Li, Thermal Conductivity of Multiwalled Carbon Nanotubes, *Physical Review B 66* (**2002**) 165440–6.

[22] T. Miao, S. Shi, S. Yan, W. Ma, X. Zhang, K. Takahashi, T. Ikuta, Integrative Characterization of the Thermoelectric Performance of an Individual Multiwalled Carbon Nanotube, *Journal of Applied Physics 120* (**2016**) 124302–6.

[23] C. T. White, D. H. Robertson, J. W. Mintmire, Helical and Rotational Symmetries of Nanoscale Graphitic Tubules, *Physical Review B 47* (**1993**) 5485–5488.

[24] N. Hamada, S. I. Sawada, A. Oshiyama, New One-dimensional Conductors: Graphitic Microtubules, *Physical Review Letters 68* (**1992**) 1579–1581.

[25] R. Dovesi, R. Orlando, A. Erba, C. M. Zicovich-Wilson, B. Civalleri, S. Casassa, L. Maschio, M. Ferrabone, M. De La Pierre, P. e. a. D'Arco, CRYSTAL14: a Program for the Ab Initio Investigation of Crystalline Solids, *International Journal of Quantum Chemistry 114* (**2014**) 1287–1317.

[26] J. P. Perdew, K. Burke, M. Ernzerhof, Generalized Gradient Approximation Made Simple, *Physical Review Letters 18* (**1996**) 3865–3868.

[27] A. D. Becke, Density-functional Thermochemistry. III The Role of Exact Exchange, *The Journal of Chemical Physics 98* (**1993**) 5648–5652.

[28] S. Grimme, Semiempirical GGA-type Density Functional Constructed with a Long-range Dispersion Correction, *Journal of Computational Chemistry 27* (**2006**) 1787–1799.

[29] R. Dovesi, M. Causa, R. Orlando, C. Roetti, V. R. Saunders, Ab Initio Approach to Molecular Crystals: a Periodic Hartree-Fock Study of Crystalline Urea, *The Journal of Chemical Physics 92* (**1990**) 7402–7411.

[30] R. Dovesi, V. R. Saunders, C. Roetti, R. Orlando, C. M. Zicovich-Wilson, F. Pascale, B. Civalleri, K. Doll, N. M. Harrison, I. J. B. et al, CRYSTAL17 User's Manual, Università di Torino, Torino, **2017**.

[31] F. Pascale, C. M. Zicovich-Wilson, F. López Gejo, B. Civalleri, R. Orlando, R. Dovesi, The Calculation of the Vibrational Frequencies of Crystalline Compounds and its Implementation in the CRYSTAL Code, *Journal of Computational Chemistry 25* (**2004**) 888–897.

[32] C. M. Zicovich-Wilson, F. Pascale, C. Roetti, V. R. Saunders, R. Orlando, R. Dovesi, Calculation of the Vibration Frequencies of $\alpha$-quartz: the Effect of Hamiltonian and Basis Set, *Journal of Computational Chemistry 15* (**2004**) 1873–81.

[33] C. M. Zicovich-Wilson, F. J. Torres, F. Pascale, L. Valenzano, R. Orlando, R. Dovesi, Ab initio Simulation of the IR Spectra of Pyrope, Grossular and Andradite, *Journal of Computational Chemistry 29* (**2008**) 2268–2278.

[34] M. Lundstrom, *Fundamentals of Carrier Transport*, Cambridge University Press, U.K., **2009**.

[35] G. Sansone, A. Ferretti, L. Maschio, Ab Initio Electronic Transport and Thermoelectric Properties of Solids from Full and Range-separated Hybrid Functionals, *The Journal of Chemical Physics 147* (**2017**) 114101.

[36] S. Boys, F. Bernardi, The Calculation of Small Molecular Interactions by the Differences of Separate Total Energies. Some Procedures with Reduced Errors, *Molecular Physics 19* (**1970**) 553–566.

[37] E. Davidson, D. Feller, Basis Set Selection for Molecular Calculations, *Chemical Reviews 86* (**1986**) 681–696.

[38] M.-F. Yu, M. J. Dyer, J. Chen, D. Qian, W. K. Liu, R. S. Ruoff, Locked Twist in Multiwalled Carbon-nanotube Ribbons, *Physical Review B 64* (**2001**) 241403–4.

[39] Y.-K. Kwon, D. Tománek, Electronic and Structural Properties of Multiwall Carbon Nanotubes, *Physical Review B 58* (**1998**) R16001–R16004.

[40] Y. Saito, T. Yoshikawa, S. Bandow, M. Tomita, T. Hayashi, *Interlayer spacings in carbon nanotubes*, *Physical Review B 48* (**1993**) 1907–1909.

[41] I. Razado-Colambo, J. Avila, D. Vignaud, S. Godey, X. Wallart, D. P. Woodruf, M. C. Asensio, Structural Determination of Bilayer Graphene on SiC(0001) Using Synchrotron Radiation Photoelectron Difraction, *Scientific Reports 8* (**2018**) 1–10.

[42] R. Saito, R. Matsuo, T. Kimura, G. Dresselhaus, M. S. Dresselhaus, Anomalous Potential Barrier of Double-wall Carbon Nanotube, *Chemical Physics Letters 348* (**2001**) 187–193.

[43] J. L. Blackburn, A. J. Ferguson, C. Cho, J. C. Grunlan, Carbon-Nanotube-Based Thermoelectric Materials and Devices, *Advanced Materials 30* (**2018**) e1704386–35.

[44] P. Kim, L. Shi, A. Majumdar, P. L. McEuen, Thermal Transport Measurements of Individual Multiwalled Nanotubes, *Physical Review Letters 87* (**2001**) 215502–4.

[45] N. Chiodarelli, O. Richard, H. Bender, M. Heyns, S. D. Gendt, G. Groeseneken, P. M. Vereecken, Correlation between Number of Walls and Diameter in Multiwall Carbon Nanotubes Grown by Chemical Vapor Deposition, *Carbon 50* (**2012**) 1748–1752.

[46] J. Kastner, T. Pichler, H. Kuzmany, S. Curran, W. Blau, D. N. Weldon, M. Delamesiere, S. Draper, H. Zandbergen, Resonance Raman and Infrared Spectroscopy of Carbon Nanotubes, *Chemical Physics Letters 237* (**1994**) 53–58.

[47] A. Dasmahapatra, L. E. Daga, A. J. Karttunen, L. Maschio, S. Casassa, Key Role of Defects in Thermoelectric Performance of TiMSn (M = Ni, Pd, and Pt) Half-Heusler Alloys, *The Journal of Physical Chemistry C 124* (**2020**) 14997–15006.

[48] Y. Nakai, K. Honda, K. Yanagi, H. Kataura, T. Kato, T. Yamamoto, Y. Maniwa, Giant Seebeck Coefficient in Semiconducting Single-wall Carbon Nanotube Film, *Applied Physics Express 7* (**2014**) 025103–4.

[49] A. D. Avery, B. H. Zhou, J. Lee, E.-S. Lee, E. M. Miller, R. Ihly, D. Wesenberg, K. S. Mistry, S. L. Guillot, B. L. Zink, Y.-H. Kim, J. L. Blackburn, A. J. Ferguson, Tailored Semiconducting Carbon Nanotube Networks with Enhanced Thermoelectric Properties, *Nature Energy 1* (**2016**) 16033–9.

[50] N. T. Hung, A. R. T. Nugraha, E. H. Hasdeo, M. S. Dresselhaus, R. Saito, Diameter Dependence of Thermoelectric Power of Semiconducting Carbon Nanotubes, *Physical Review B 92* (**2015**) 165426–7.

[51] J. Hone, I. Ellwood, M. Muno, A. Mizel, M. L. Cohen, A. Zettl, A. G. Rinzler, R. E. Smalley, Thermoelectric Power of Single-Walled Carbon Nanotubes, *Physical Review Letters 80* (**1998**) 1042–1045.

[52] K. Yanagi, S. Kanda, Y. Oshima, Y. Kitamura, H. Kawai, T. Yamamoto, T. Takenobu, Y. Nakai, Y. Maniwa, Tuning of the Thermoelectric Properties of One-dimensional Material Networks by Electric Double Layer Techniques Using Ionic Liquids, *Nano Letters 14* (**2014**) 6437–6442.